

## Transport of north China air pollution by midlatitude cyclones: Case study of aircraft measurements in summer 2007

Aijun Ding,<sup>1</sup> Tao Wang,<sup>1,2</sup> Likun Xue,<sup>1,3</sup> Jian Gao,<sup>1,3</sup> Andreas Stohl,<sup>4</sup> Hengchi Lei,<sup>5</sup> Dezhen Jin,<sup>6</sup> Yu Ren,<sup>1</sup> Xuezhong Wang,<sup>7</sup> Xiaolin Wei,<sup>1</sup> Yanbin Qi,<sup>6</sup> Jian Liu,<sup>6</sup> and Xiaoqing Zhang<sup>5</sup>

Received 27 August 2008; revised 6 February 2009; accepted 17 February 2009; published 22 April 2009.

[1] Warm conveyor belts (WCBs) and frontal activity play important roles in the long-range transport of air pollutants by lifting them from the planetary boundary layer (PBL) into the free troposphere (FT) in midlatitudes. In summer 2007, an aircraft study was carried out in northeast (NE) China in order to understand the role of midlatitude cyclones in air pollution transport in north and east China in warm seasons. During a flight on 27 June, high concentrations of ozone and related trace gases were observed, with maximum concentrations ( $O_3 \sim 140$  ppbv,  $SO_2 \sim 14.6$  ppbv,  $CO \sim 1185$  ppbv) recorded at an altitude of 2.6 km. In this paper we present a detailed analysis of this flight. The mesoscale meteorological model Weather Research and Forecasting (WRF) and a Lagrangian dispersion model called FLEXPART were used to aid the diagnostic analysis of the atmospheric dynamic structure and the understanding of the transport characteristics of regional and local air pollution. The flight took place in a region adjacent to a warm front associated with a weak cyclone in north China. The aircraft sampled both the WCB and warm air frontal zone of the cyclone. The simulations show that the observed high air pollution in the FT mostly originated from the North China Plain, especially the megacities Beijing and Tianjin. Their plumes were vented by a stagnant front, probably through, in part, topographic lifting by the mountains in the north, and then were quickly transported in the FT to the study region. Trajectory analysis and satellite data suggest that the observed air masses were further lifted by the WCB into the middle and upper troposphere and were exported from Asia toward North America and the Arctic.

**Citation:** Ding, A., et al. (2009), Transport of north China air pollution by midlatitude cyclones: Case study of aircraft measurements in summer 2007, *J. Geophys. Res.*, 114, D08304, doi:10.1029/2008JD011023.

### 1. Introduction

[2] The study of air pollution transport from the planetary boundary layer (PBL) into the free troposphere (FT) is of great importance for the understanding of atmospheric chemistry and climate issues, because air pollutants, including ozone, aerosols, and their precursors, can substantially change the chemical environment and radiation property of

the troposphere. The longer lifetime of these pollutants in the FT extends their impact from the regional to the continental, or even global, scale because of long-range transport [Stohl and Trickl, 1999; Donnell et al., 2001; Liu et al., 2003; Henne et al., 2005; Dickerson et al., 2007]. The major meteorological mechanisms that contribute to lifting or ventilating PBL air into the free troposphere include frontal activity, deep convection, and orographic forcing [Donnell et al., 2001; Wild and Akimoto, 2001; Vaughan et al., 2003; Henne et al., 2004]. Among these mechanisms, the frontal systems, especially the so-called warm conveyor belts (WCBs), which are associated with extratropical cyclones, are dominant in the vertical redistribution of pollution in the midlatitudes [Bethan et al., 1998; Wild and Akimoto, 2001; Miyazaki et al., 2003; Kiley and Fuelberg, 2006].

[3] Because of increasing concern about the long-range transport of air pollutants in Asia, particularly continental eastern Asia, midlatitude cyclones and their effects on pollution transport have been widely studied in recent decades [Jaffe et al., 1999, 2003; Miyazaki et al., 2003; Tsutsumi et al., 2003; Cooper et al., 2004; Liang et al.,

<sup>1</sup>Department of Civil and Structural Engineering, Hong Kong Polytechnic University, Hong Kong, China.

<sup>2</sup>Also at Chinese Research Academy of Environmental Sciences, Beijing, China.

<sup>3</sup>Also at Environmental Research Institute, Shandong University, Jinan, China.

<sup>4</sup>Norwegian Institute for Air Research, Kjeller, Norway.

<sup>5</sup>Institute of Atmospheric Physics, Chinese Academy of Science, Beijing, China.

<sup>6</sup>Weather Modification Office, Jilin Provincial Meteorological Bureau, Changchun, China.

<sup>7</sup>Chinese Research Academy of Environmental Sciences, Beijing, China.

2004; *Mari et al.*, 2004; *Oshima et al.*, 2004; *Dickerson et al.*, 2007]. Some studies have shown that strong WCBs can lift Asian pollution plumes into the upper troposphere, where they can be transported rapidly to North America [*Cooper et al.*, 2004] and even Europe [*Stohl et al.*, 2003, 2007]. Modeling studies have also shown that convection plays an important role in air pollution lifting, especially in warm seasons [*Chatfield and Crutzen*, 1984; *Wild and Akimoto*, 2001; *Liang et al.*, 2004]. However, previous aircraft measurement studies in Asia have mainly been conducted in cold seasons and there were relatively few investigations of the detailed mechanisms of WCBs and convection and their roles on transporting air pollution from China in summer.

[4] North China Plain (NCP), which includes the Beijing and Tianjin city clusters and many other cities in the flat region of central eastern China, experiences serious air pollution including photochemical ozone pollution owing to high population density and intense industrial activities in the region. For example, ozone concentrations of 200–300 ppbv have been observed in urban and regional plumes in a rural area near Beijing [*Wang et al.*, 2006]. The high and increasing ozone concentrations in the lower troposphere over Beijing have been shown by analysis of MOZAIC (Measurement of Ozone and Water Vapor by Airbus In-Service Aircraft) data collected during 1995–2005 [*Ding et al.*, 2008]. Ozone pollution has also been observed at the summit of Mount Tai (1534 m above sea level) during summer [*Gao et al.*, 2005; *Li et al.*, 2007]. However, large-scale synoptic processes and their roles in the long-range transport of the regional pollution in summer are not yet well understood, although some studies indicate that these processes frequently occur. For instance, an early diagnostic study by *Chen et al.* [1991] suggested that in summer there was a very high frequency of cyclogenesis and cyclone events over the NCP and Mongolia. On the basis of climatological trajectory analysis, *Eckhardt et al.* [2004] and *Stohl* [2001] also found a high frequency of WCB events over the NCP and northeast (NE) China, which is consistent with the distribution of cyclone events given by *Chen et al.* [1991]. These results reveal that cyclones and the accompanied frontal activity probably play an important role in the export of photochemically aged air pollution from this region, and that NE China, because it is downwind of that region, is a particularly well suited area to carry out further studies of these transport mechanisms and the regional impact of NCP plumes.

[5] In the summer of 2007, we conducted an aircraft measurement campaign in the province of Jilin in NE China for China's National Basic Research Program (also known as the "973 Program") on acid rain pollution and control. We specially designed a flight, under a typical condition of a midlatitude cyclone in late June, to investigate the vertical distribution of ozone and related trace gases as well as aerosols in the low troposphere, and the role of WCBs and convection in PBL-FT air pollution transport in this and upwind regions. We present herein a detailed analysis of the observed episode using mesoscale meteorological modeling and Lagrangian particle dispersion simulation. We describe the experiments and modeling tools in sections 2 and 3, respectively, and present the results of the simulations and discussion of the dynamic structure and transport mecha-

nisms for this case in section 4. Finally, section 5 gives the conclusions.

## 2. Experiments

[6] We conducted aircraft measurements of trace gases, aerosols, and cloud water from June to July 2007 in the province of Jilin in NE China. This campaign aimed to characterize the photochemistry and gas-particle-cloud interaction and their impacts on acid rain in this region, and to study the vertical distribution of air pollutants and PBL-FT exchange under typical synoptic conditions.

[7] A Yun-12 aircraft of the Jilin Weather Modification Office was used for the study. This twin-engine turboprop aircraft is similar to a Twin Otter. The aircraft campaign was conducted out of Changchun (the capital of Jilin, with a population of 7 million) and confined within the province (see Figure 1). The airport is located in the northwest (generally upwind direction) of the city, and is about 280 km from the city of Shenyang (population: 7 million), the capital of Liaoning and one of the largest industrial cities in NE China with relatively high levels of anthropogenic emissions (see the black spot in area 2 of Figure 1a). The airport is located about 800 km to the northeast of Beijing. In summer, the surface air masses in general come from either Mongolia or Siberia in the northwest, and from the ocean and coastal region in the south/southwest. Under the latter condition, the air is relatively humid and polluted.

[8] The sampling inlet was mounted at the bottom of the airframe with an aft-facing inlet connected to gas analyzers, while an isokinetic forward-facing inlet fed the aerosol instruments. O<sub>3</sub> was measured with a UV photometric analyzer (TEI-49), CO was measured with a nondispersive infrared analyzer (API-300), SO<sub>2</sub> was measured with a pulsed UV fluorescence analyzer (TEI-43C TL), and the aerosol scattering coefficient was measured with a commercial integrating nephelometer (Eco Tech, M9003), which detects the light scattering coefficient ( $B_{sp}$ ) at 520 nm. The 5-s trace-gas data were collected by a data logger, and the time resolution of  $B_{sp}$  was 1 min. In addition, meteorological parameters including the air temperature and pressure, liquid water content (LWC, measured by the Forward Scattering Spectrometer Probe FSSP-100 of PMS Inc.), and global positioning system data were also recorded. All trace gas instruments were calibrated at the ground base and at different altitudes on several selected flights. During the campaign, we also collected 95 VOC canister samples, which were analyzed by Professor Donald Blake's laboratory at the University of California, Irvine, after the campaign. The CO canister results show good agreement with our online CO measurements.

[9] Sixteen flights were carried out in several typical weather conditions. In this paper, we focus on a flight carried out on 27 June 2007, a special case designed to understand the distribution and transport of air pollutants associated with midlatitude cyclones. A detailed analysis of the synoptic conditions is given in section 4.2, and here we give a brief description of the flight route shown in Figure 1b. Because of aviation control restrictions in this area, the flight altitudes were confined to below 3 km during the whole flight. The aircraft ascended from the airport and made an anticlockwise flight in the middle of the province

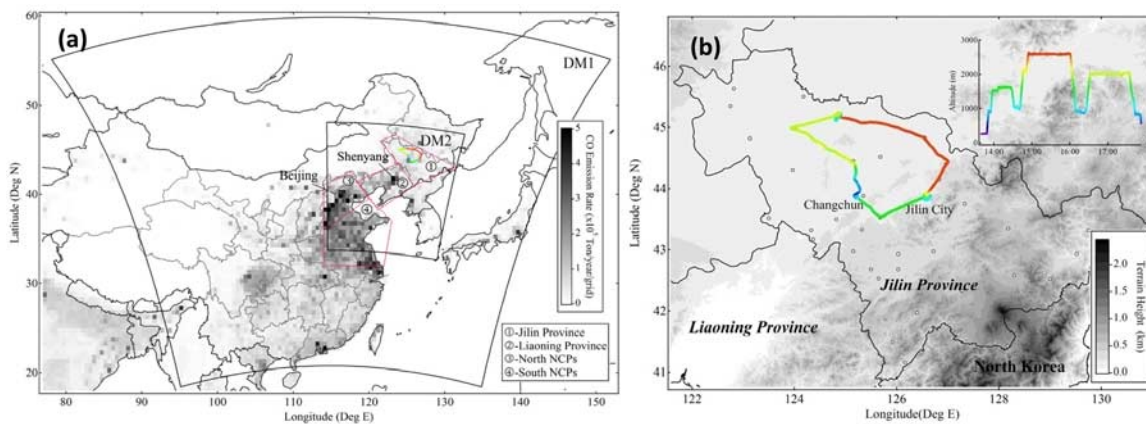


**Figure 1.** (a) Map showing the anthropogenic emission of CO and the study area and (b) the flight track of 27 June 2006 on a topographic map. Note that the CO emission rate was obtained from [http://www.cgrer.uiowa.edu/EMISSION\\_DATA\\_new/index\\_16.html](http://www.cgrer.uiowa.edu/EMISSION_DATA_new/index_16.html). Grid size is  $0.5^\circ$  by  $0.5^\circ$ . The color along the flight route indicates altitude. DM1 and DM2 in Figure 1a represent the respective WRF coarse and fine domains. Four typical areas (1–4) are identified for the late source analysis.

at an altitude of around 2.6 km (about 2.4 km above ground level). To capture the air pollutant distributions around the top of the PBL, the aircraft descended to about 800 m over a petrochemical city, Jilin, in the south and another small city, Fuyu, in the north (see the flight altitude given in Figure 1b). The flight was carried out from 1330 to 1750 LT on 27 June and covered a total distance of about 700 km.

### 3. Modeling Tools and Methodology

#### 3.1. Mesoscale Meteorological Simulation and Evaluation

[10] We employed the Weather Research and Forecasting (WRF) model to conduct mesoscale meteorological simulations to help in the understanding of the transport mechanisms during the episode. The WRF modeling system is a next-generation mesoscale forecast and simulation system, which is a fully compressible and nonhydrostatic Euler model [Skamarock *et al.*, 2005]. In this work, we used WRF version 2.2 with the Advanced Research WRF dynamics solver. The model was run in two two-way nested domains, covering east Asia and north and NE China (see Figure 1a), with a horizontal grid size of 30 km and 10 km, respectively. Both domains have 37 terrain-following vertical sigma levels. The NCEP final analyses data, with  $1^\circ \times 1^\circ$  horizontal resolution, 26 vertical levels, and six-hourly temporal resolution, were used to provide the boundary and initial conditions for the WRF simulations. A Mellor-Yamada-Janjic turbulence kinetic energy scheme was used for PBL closure, and a Kain-Fritsch (new Eta) scheme was chosen for cumulus parameterization but was called every 5 min for computing efficiency. To limit forecast errors, the model was restarted (with new boundary and initial conditions) every 12 hours from 20 to 29 June 2007. Finally, the simulations generated a meteorological database with a high temporal resolution (5 min) for further diagnostic analysis and Lagrangian simulation.

[11] To validate the WRF simulations, we compare the results with surface observations at two representative

surface observatories in Changchun and Beijing, and with the aircraft-measured parameters in Figures 2a–2c. Here, we present comparisons only for air temperature and sea level pressure for surface sites and temperature from aircraft observations with modeling output from WRF fine domain. We also compare the satellite cloud images with WRF-simulated specific humidity in section 4.2. Figure 2 suggests that the WRF simulations reproduced the overall variations in temperature and pressure during the period, such as the gradually increasing air temperature during the previous week and the drop in the sea level pressure around 25 June at the two sites, and were in good agreement with the air temperature variations along the flight track. However, notable differences still remain for some parameters, which are likely attributable to uncertainty from physical parameterization and initial/boundary conditions of meteorological models [e.g., Ding *et al.*, 2004; de Foy *et al.*, 2006].

#### 3.2. Lagrangian Particle Dispersion Simulation and Potential Source Contribution Analysis

[12] To simulate and diagnose the transport and dispersion processes for this episode, we employed a Lagrangian particle dispersion model, FLEXPART [Stohl *et al.*, 2005] (see <http://zardoz.nilu.no/~andreas/flextra+flexpart.html>). FLEXPART releases so-called tracer particles at emission sources/or receptors and calculates their trajectories using the mean winds interpolated from the meteorological input fields plus random motions representing turbulence. This model has been widely used in the analysis of data for atmospheric chemistry experiments to investigate the influence of various meteorological processes on pollution transport, such as stratospheric intrusions [Cooper *et al.*, 2006], WCBs [Stohl *et al.*, 2003; Cooper *et al.*, 2004; Stohl *et al.*, 2007], and dispersion over complex terrains [de Foy *et al.*, 2006; Palau *et al.*, 2006]. A special feature of FLEXPART is the possibility to run it backward in time to produce information on the spatial distribution of sources contributing to a particular measurement [Stohl *et al.*, 2003; Seibert and Frank, 2004].

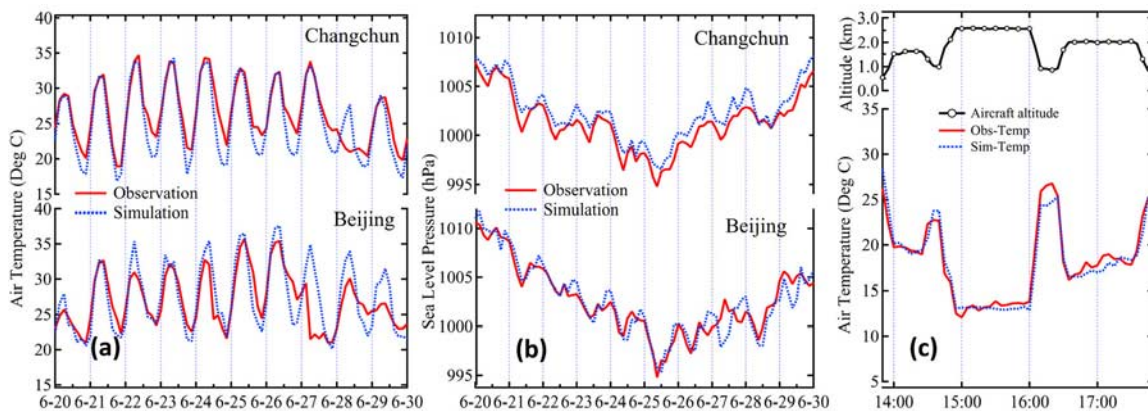


**Figure 2.** Comparison of WRF simulations with surface-observed (a) air temperature and (b) sea level pressure at Beijing and Changchun observatories from 20 to 29 June, as well as with (c) aircraft-observed temperature.

[13] In the current work, we used a modified WRF/FLEXPART model, developed by Jerome Fast of the National Center for Atmospheric Research on the basis of FLEXPART 5.0, to conduct backward Lagrangian particle simulations. The model was run in a nesting mode, on the basis of the WRF output, to obtain a high-resolution (temporal and spatial) simulation. The time step was 150 s, and the particle location and emission sensitivity fields were outputted every 10 min. Backward simulations were made from small segments, with a horizontal distance of  $0.1^\circ$  and a thickness of 200 m vertically along the flight track or from other locations of interest. For each segment, 20,000 particles were released and followed backward in time for 7 days, forming what we call a retroplume as described by Seibert and Frank [2004] and Stohl *et al.* [2003].

[14] Next, we adopted a methodology similar to that employed by Stohl *et al.* [2003, 2007] to simulate CO concentrations. For each receptor, the residence time for a thickness of 100 m above the surface was calculated and considered the “footprint” retroplume (in units of s per grid). Multiplication with the emission flux densities (in units of  $\text{ppbv s}^{-1}$ ) calculated from a 2006 emission inventory prepared by Dr. David Streets for the Intercontinental Chemical Transport Experiment (INTEX-B) mission (data were obtained from [http://www.cgcr.uiowa.edu/EMISSION\\_DATA\\_new/index\\_16.html](http://www.cgcr.uiowa.edu/EMISSION_DATA_new/index_16.html)) (see also Figure 1a) yielded a so-called potential source contribution map, which is the geographical distribution of sources contributing to the simulated mixing ratio at the receptor. The word “potential” here indicates that this sensitivity is based on transport alone, ignoring chemical and removal processes that would reduce the sensitivity. Spatial integration of the potential source contribution map gives the simulated mass mixing ratio for the flight segment. As the particle output was generated at intervals of 10 min during the 7-day backward simulation period, the timing (i.e., age) of the contributing emissions is also known. For the detailed steps of the calculation of the backward simulation, please refer to Figure 10 for an illustration. In this paper, we used this method to simulate the CO concentrations along the flight

track and diagnose the vertical structure of the CO plumes on interesting cross sections.

## 4. Results and Discussion

### 4.1. Overall Observation Results

[15] Figure 3 shows the overall time series of  $\text{O}_3$ , CO,  $\text{SO}_2$ ,  $B_{\text{sp}}$ , and flight altitude for this episode. It can be seen that during the entire flight, the study region suffered from high loads of photochemical pollution, with averaged  $\text{O}_3$ , CO, and  $\text{SO}_2$  of about 100, 500, and 6 ppbv, respectively. These results, especially  $\text{O}_3$  concentrations, are much higher than those observed downwind of Asia during the TRACE-P study [Jacob *et al.*, 2003; Jaegle *et al.*, 2003; Crawford *et al.*, 2004], which was conducted over the remote northwest Pacific in spring [Jacob *et al.*, 2003]. This suggests a lot of mixing and dilution in the Asian boundary layer, though our study was carried out in summer and in a region of higher latitude compared to the TRACE-P study.

[16] Regarding the detailed variations of air pollutants during the flight, near-uniform  $\text{O}_3$  and CO during the first 1.5 hours were noted, even when the aircraft descended to an altitude of 800 m over the city of Jilin. However, a notable drop in  $\text{SO}_2$  was observed, from about 10 ppbv to 4 ppbv, when the aircraft took off from the airport and ascended to 1500 m, which is a typical PBL profile of  $\text{SO}_2$  in this region. It is interesting that when the aircraft ascended to an altitude of 2.6 km and flew northwestward from 1500 to 1600 LT, the concentrations of trace gases rose to even higher levels than those measured in the PBL. It can also be seen that the air pollutants dropped to relatively low values at 1510 LT (CO  $\sim$  202 ppbv,  $\text{SO}_2$   $\sim$  1.2 ppbv,  $\text{O}_3$   $\sim$  63 ppbv), but peaked at 1530 LT ( $\text{O}_3$ , CO, and  $\text{SO}_2$  were up to 140, 1185, and 14.6 ppbv, respectively). The distance between the locations where the background and polluted air parcels were captured is about 60 km. Figure 3 also shows that a broad peak in the air pollutants, especially in  $B_{\text{sp}}$ , was observed after the aircraft descended into the PBL around Fuyu from 1600 to 1640 LT. After 1640 LT, when the aircraft flew a constant-altitude leg around 2 km, concentrations of air pollutants dropped to relatively low

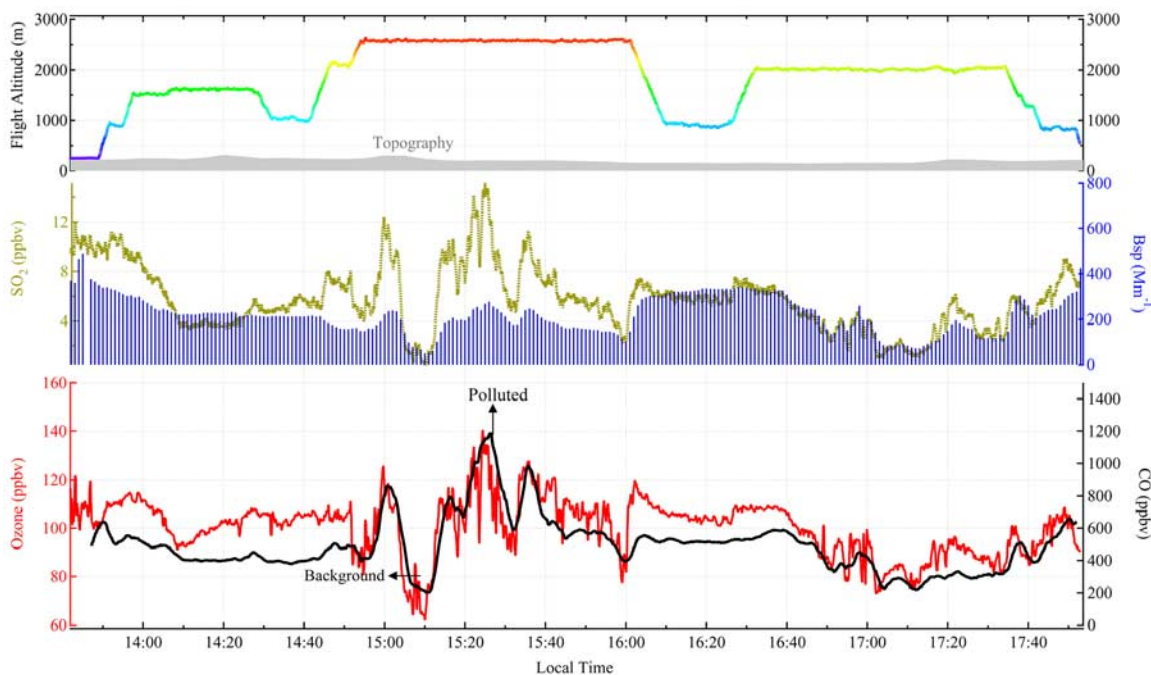


**Figure 3.** Time series of O<sub>3</sub>, CO, SO<sub>2</sub>, B<sub>sp</sub>, and flight altitude during the flight on 27 June 2007.

levels and then gradually increased as the plane descended before landing.

[17] The time series in Figure 3 show positive correlations between these air pollutants. To give a clearer picture, Figures 4a–4c present the scatterplots of O<sub>3</sub> versus CO, O<sub>3</sub> versus SO<sub>2</sub>, and SO<sub>2</sub> versus B<sub>sp</sub>. Figures 4a–4c were color-coded with the flight altitude. Figures 4a and 4b show that O<sub>3</sub> had a strong positive correlation with the primary trace gases CO and SO<sub>2</sub>, suggesting that the O<sub>3</sub> episode in this study was due to anthropogenic sources. The slope of 0.05 for the O<sub>3</sub>/CO ratio was close to those measured at

Mt Tai and at a polluted rural site, Lin'an (0.08) in eastern China [Wang *et al.*, 2001; Gao *et al.*, 2005], but much lower than the O<sub>3</sub>/CO slope ( $\sim 0.3$ ) observed downwind of North America [Parrish *et al.*, 1993; Chin *et al.*, 1994]. The lower O<sub>3</sub>/CO ratios in China are in part owing to the strong emission of CO relative to NO<sub>x</sub> [Wang *et al.*, 2001; Streets *et al.*, 2006]. SO<sub>2</sub> shows a better correlation with O<sub>3</sub> than does CO, especially at a high altitude (in red). The scatterplot of B<sub>sp</sub> and SO<sub>2</sub> suggests a positive correlation between SO<sub>2</sub> and secondary sulfate aerosols that generally have a good correlation with B<sub>sp</sub> [Delene and Ogren, 2002]. It is

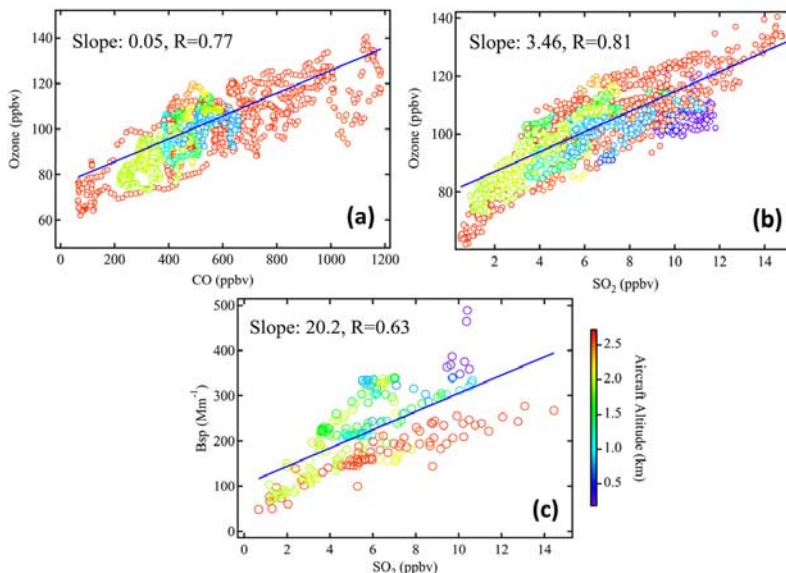


**Figure 4.** Correlations between species during the aircraft study: (a) O<sub>3</sub> versus CO, (b) O<sub>3</sub> versus SO<sub>2</sub>, and (c) B<sub>sp</sub> versus SO<sub>2</sub>.

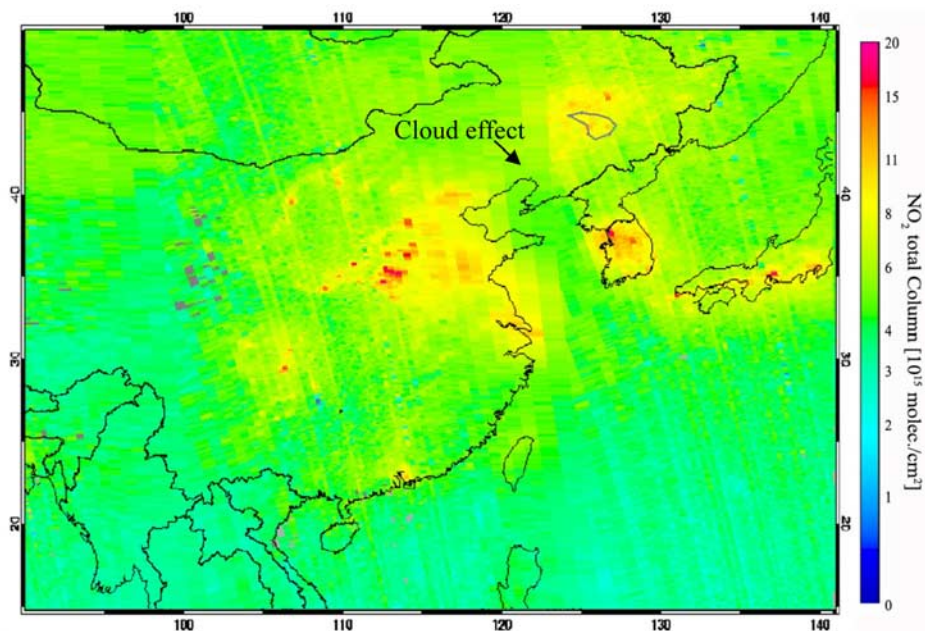


**Figure 5.** OMI-retrieved  $\text{NO}_2$  column in east Asia on 27 June 2007. Note that the OMI overpass time is about 1330 LT. Data source is the Tropospheric Emission Monitoring Internet Service available at <http://www.temis.nl>.

worthwhile to note that the slope of the  $B_{\text{sp}}/\text{SO}_2$  ratio is clearly dependent on altitude, i.e., a higher slope is associated with a lower altitude. This difference could be due to the hygroscopic effect of relative humidity on aerosol light scattering [Malm *et al.*, 2003] or the influence of clouds. The measured liquid water content shows that the aircraft encountered some clouds when the aircraft took a PBL flight over Fuyu, corresponding with the broad peak of  $B_{\text{sp}}$  in Figure 3.

[18] The high concentration of primary and secondary air pollutants and positive correlation between them suggest that the aircraft sampled photochemically aged plumes. To obtain a regional picture of the air pollution distribution, Figure 5 shows the OMI satellite-retrieved  $\text{NO}_2$  columns (data were obtained from the Tropospheric Emission Monitoring Internet Service at <http://www.temis.nl/>). A comparison of the patterns of  $\text{NO}_2$  distribution with the CO emission inventory in Figure 1a reveals that the flight was carried out in a regional plume in NE China, which was transported into the region because emissions in the study area are relatively low. The low  $\text{NO}_2$  column between the study region and the NCP (see Figure 5) was probably due to the influence of clouds in this area, corresponding with the cloud images shown in Figure 6.

#### 4.2. Synoptic Processes and Airstream Patterns

[19] Using WRF simulation output and satellite images, we present a detailed analysis of the synoptic processes and general atmospheric circulation within 2 to 3 days of the aircraft study. Figures 6a–6c present the composite satellite IR images and sea level pressure contours, with the frontal analysis superimposed, at 2000 LT on 25 June, 1600 LT on 27 June, and 0000 LT on 28 June 2007, respectively; and Figures 6d–6f show the 500 hPa specific humidity (unit:  $\text{g g}^{-1}$ ), and wind vectors corresponding with Figures 6a–6c.

[20] It can be seen that at 2000 LT on 25 June, i.e., 40 hours before our aircraft study commenced, a deep midlatitude cyclone was located over eastern Siberia (centered at  $120^\circ\text{E}$ ,  $55^\circ\text{N}$ ), with a relatively stationary cold/warm front extending from NE China southwestward to the northern edge of the NCP. The satellite image clearly shows embedded convective clouds along the front, and the 500 hPa specific humidity field (Figure 6d) consistently shows a moist band over the front, revealing strong vertical venting in this region. An examination of the hourly satellite images suggests that such a frontal cloud band existed over the north of China from noontime 25 June to early morning 26 June. In later sections, we discuss how the long existence of convection there could play an important role in transporting air pollution from the NCP.

[21] The strong midlatitude cyclone moved eastward in the following two days, leaving a tail-like cloud band over northern China, and developed into a weak cyclone on 27 June, i.e., during the aircraft study period (see Figures 6b and 6e). At the same time, another cyclone was located further south, in east China. The aircraft route given in Figure 6 suggests that our aircraft measurements were taken in a warm sector adjacent to and partly crossing the warm front of the weak cyclone in the north. It should be pointed out that WCBs were often directly defined from satellite image alone [Carlson, 1998; Cooper *et al.*, 2004], which works very well for cold season WCBs. However, it is difficult to identify WCB circulations from the cloud image given in Figure 6b. Nevertheless, the T-shaped distribution of the specific humidity in Figure 6e reveals that a WCB-like circulation (i.e., WCB1) extended from the warm sector to the aircraft study area and overran the warm front. In fact, Kiley and Fuelberg [2006] pointed out the importance of convection in shaping the WCB of a summertime cyclone. In the case of a rather weak cyclone such as that studied

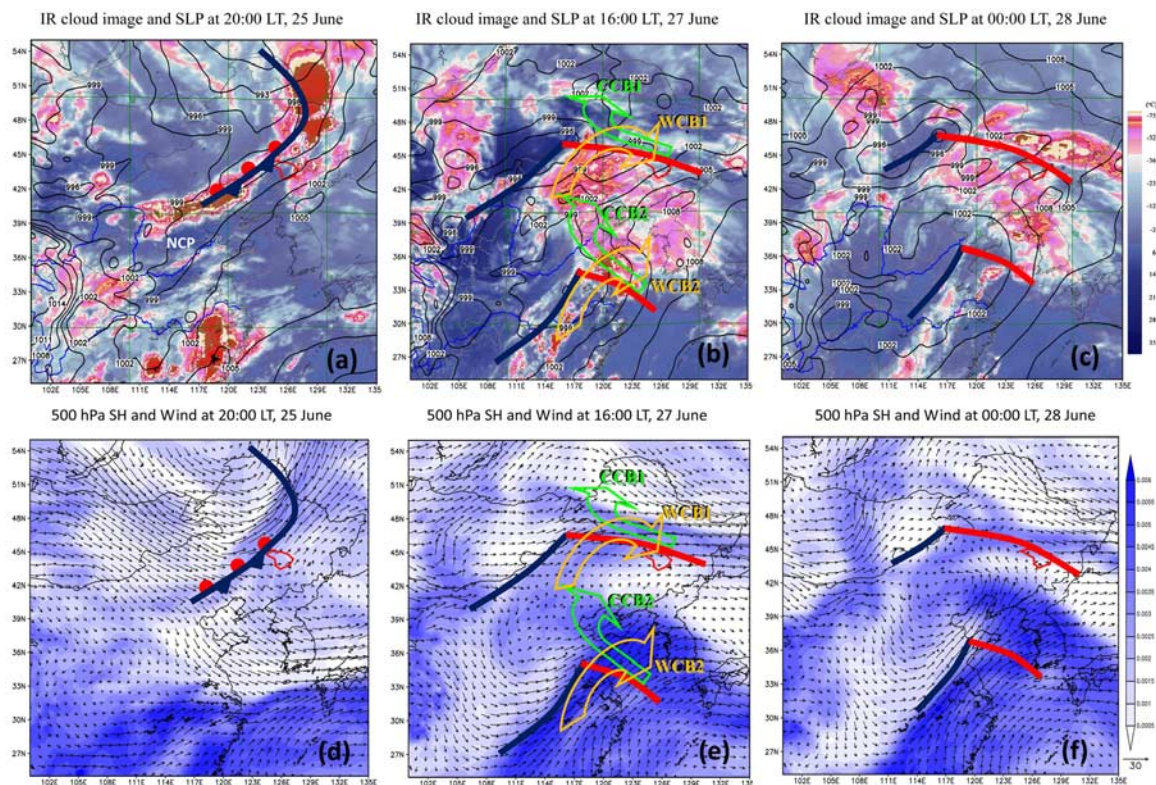


**Figure 6.** Distribution of sea level pressure and FY-2 satellite IR cloud image at (a) 2000 LT on 25 June, (b) 1600 LT on 27 June, and (c) 0000 LT on 28 June, as well as (d–f) specific humidity (units of  $\text{g g}^{-1}$ ) and wind vectors at 500 hPa corresponding with Figures 6a–6c. Note that the thin red line is the aircraft route, and the blue and red bold lines show the surface cold fronts and warm fronts, respectively.

here, this makes it relatively difficult to clearly identify the WCB from the cloud features alone. Figure 6c suggests that in the following eight hours, WCB-induced clouds, showing a clockwise band overrunning the warm front, existed in the east of the study region. This pattern is similar to the circulation in the classical conceptual model of WCBs [e.g., Carlson, 1998; Cooper *et al.*, 2001; Schultz, 2001; Kiley and Fuelberg, 2006]. Associated with the WCBs and embedded convection, rainfall was reported in this region on 28 June with more rain in the afternoon.

[22] Figures 6b and 6e also suggest that on 27 June the cold conveyor belt circulation (CCB2) of the cyclone in the south probably joined with WCB1 in the north, transporting air to the study region. Another important issue is that in Figure 6 the 500 hPa specific humidity distributions perfectly agree with the satellite cloud images, providing further evidence that the WRF simulations captured the major synoptic processes and vertical motions during the period.

[23] To give a clear picture about the airstreams associated with cyclones and help identify what airstreams our aircraft had captured, we calculated 48-hour three-dimensional backward and 48-hour forward trajectories for a matrix of points over the study region. Figures 7a–7c give the trajectories (96 hours in total), ending/starting at 1600 LT on 27 June for the matrix at the altitudes of 500 m, 1500 m, and 2500 m, respectively. The trajectories were calculated using the Hybrid Single-Particle Lagrangian Integrated Trajectory model (HYSPLIT 4, see [\[www.arl.noaa.gov/ready/hysplit4.html\]\(http://www.arl.noaa.gov/ready/hysplit4.html\)\) driven with the nested hourly WRF output. A strong ascent by about 4–5 km after the sampling is revealed by the trajectories. This strong ascent and increasing potential temperature and decreasing specific humidity \(not shown here\) are consistent with the criteria adopted to identify WCBs using the Lagrangian trajectory method employed by Wernli and Davies \[1997\] and Stohl \[2001\] and confirm that the WCB lifting led to precipitation. The trajectories for the different altitudes also suggest a different air parcel history in the previous two days: the air masses at 500 m were transported slowly from the ocean east of the NCP \(i.e., the Bohai and Huanghai Seas\), whereas those at a higher altitude were transported quickly from the west after descending over the northern part of the NCP, including over Beijing. It is worth noting that the trajectories show embedded convection \(see dashed circles in Figure 7b\) occurred north of NCP \( \$\sim 116^\circ\text{E}\$ \) and in the east of the study region \( \$\sim 130^\circ\text{E}\$ \). We will later discuss the role of pollution venting in the NCP.](http://</a></p>
</div>
<div data-bbox=)

#### 4.3. Planetary Boundary Layer Structure and Air Pollution Transport Mechanisms

[24] Because our flight sampled air in a small region adjacent to a warm front and at a relatively low altitude, the analysis of the structure in the low troposphere is important for the identification of the exact locations of the sampled plumes and the understanding of the transport mechanisms for this case. Therefore, we analyzed the WRF output and in

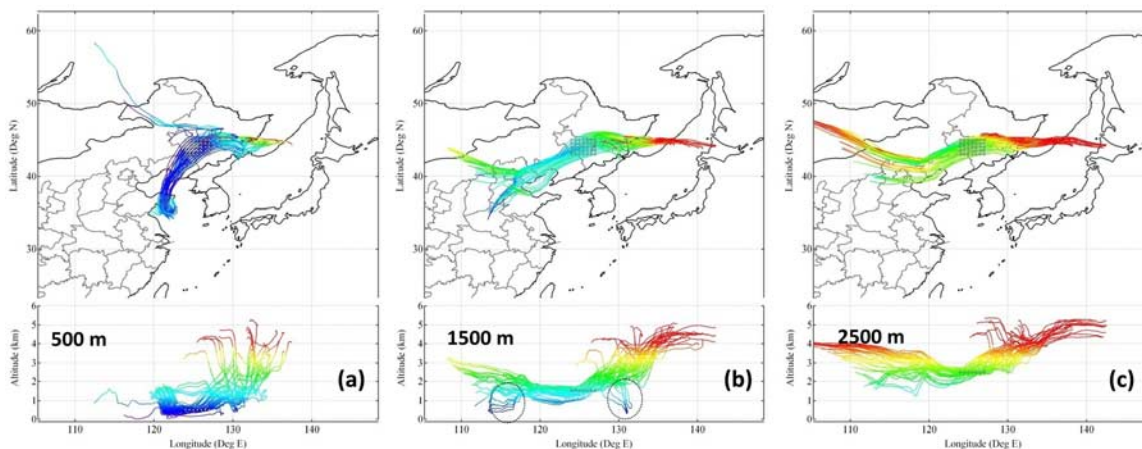


**Figure 7.** The 48-hour backward and 48-hour forward trajectories ending/starting at the matrix of points at altitudes of (a) 500 m, (b) 1500 m, and (c) 2500 m over the aircraft study area at 1600 LT on 27 June. Note that trajectories were colored with altitude (see left axis in bottom panels), and dashed open circles show convection.

Figure 8 present the vertical cross section of the physical parameters in the low troposphere (below 4 km), i.e., a time-dependent vertical structure, for a curtain along the flight. Here, the potential temperature ( $\theta$ ) contour is color-coded, and RH is shown as a brown dashed line. The WRF-predicted PBL height (i.e., mixing height) is given as a bold white line. The altitude of the flight is shown as a thin red line. To show the location of clouds during the flight, the LWC data measured by FSSP-100 are marked as white solid circles.

[25] Figure 8 shows that the PBL height was around 1.8 km (topography is about 200 m) during the beginning and ending stages, but increased up to about 2.5 km during 1510–1540 LT and dropped sharply to about 800 m during 1550–1710 LT when the aircraft flew in the north. The relatively low PBL height in the north corresponded with the location of the warm front, beneath which was relatively cold air. The highest PBL height up to 2.6 km around 1530 LT was due to the lifting over the front. Some studies [Taylor

and Guymer, 1983; e.g., Carlson, 1998] have identified the same characteristics, such as the elevated mixed layer, in the warm air frontal zone (WAFZ).

[26] An examination of Figure 8 also suggests that over the front  $\theta$  had an elevated layer, with moist/cloudy air extending up to 3.5 km (see the gray dashed line). This layer over the warm front corresponded with WAFZ defined by Taylor and Guymer [1983]. The WAFZ together with the upper WCB circulations, which turn clockwise over this region, were important for the PBL-FT transport and further lifting of air pollution in the region.

[27] Taking Figure 8 together with Figure 3 provides a rough understanding of the observed variation in air pollution. Of the two extreme cases, the background air parcel (at 1510 LT) is related to a dry intrusion (see the yellow arrow in Figure 8) carrying background air masses from the upper level, and the polluted one (at 1530 LT) seems to be due to the well-mixed PBL air (see the higher PBL height). However, later analysis demonstrates that it corresponds

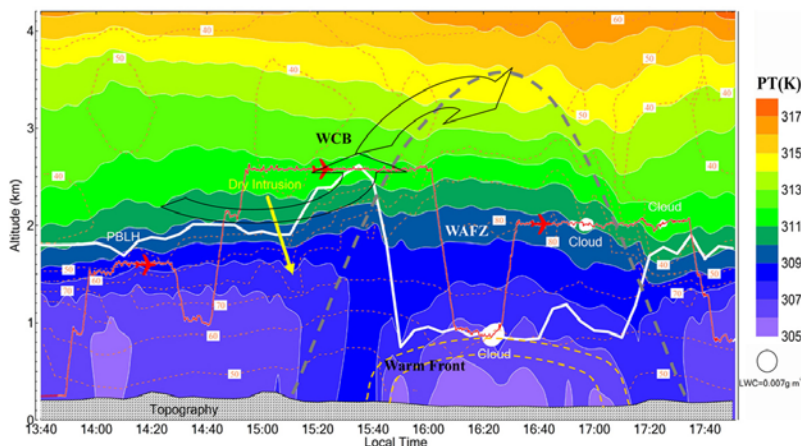


**Figure 8.** Potential temperature (rainbow color-coded), RH (brown dashed line), and PBL height (bold white line) on the curtain along the flight track in the low troposphere. White solid circles along the flight track (red line) show the measured LWC data. WAFZ, warm air frontal zone.

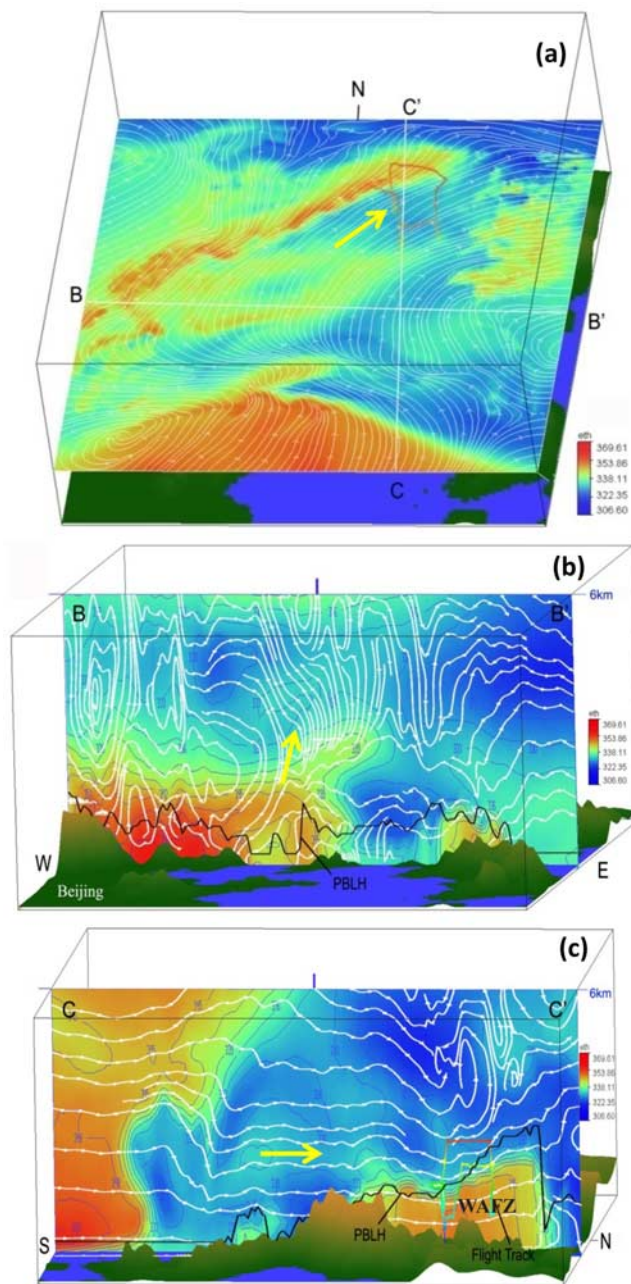


**Figure 9.** (a) Wind streams ( $u, v$ ) and equivalent potential temperature ( $\theta_e$ ) at an altitude of 2 km; (b) west–east vertical cross section of wind streams ( $u, w$ ),  $\theta_e$ , and PBLH at  $40^\circ\text{N}$  (i.e.,  $BB'$  line in Figure 9a); and (c) south–north vertical cross section of wind streams ( $v, w$ ),  $\theta_e$ , and PBL height at  $125^\circ\text{E}$  (i.e., line  $CC'$  in Figure 9a) at 1500 LT on 27 June 2007. Note: The vertical altitude in the 3-D box is 6 km. Here the  $w$  components are multiplied by 10 to show the vertical motion clearly. Yellow arrows denote the direction of wind flows.

with the frontal transport of regional pollution. It should be pointed out that although the air was moist and close to saturation, clouds had not yet formed near the plume section of the flight, but cloud formation in this mass commenced soon after the flight (see Figure 6c), as the air mass was lifted rapidly (see Figure 7).

[28] To give a three-dimensional view of the atmospheric dynamics during the experiment, we present the horizontal and vertical cross sections of the wind streams and their equivalent potential temperature ( $\theta_e$ ) at 1500 LT in Figures 9a–9c. The  $\theta_e$  (see the computation method given by Bolton [1980]) is a good tracer to study lifting warm air advection and moisture advection in the atmosphere because it always increases with increasing temperature and moisture content [Holton, 2004]. Figure 9a clearly shows that a high  $\theta_e$  value existed over the mountains in the north of the NCP and extended to the northeast, corresponding with the convergence belt over the warm front to the north of our study region. The vertical structure given in Figure 9b shows strong updrafts from the south and southeast coastal regions (see the tongue-like high  $\theta_e$  belt). Because the increase of  $\theta_e$  with altitude can produce convective stability [Luke et al., 1992; Ryan et al., 1992], these results reveal that convection, especially dry convection (with no/less cloud during the flight), could be important in venting local PBL air pollutants in this region for this case. The distribution of  $\theta_e$  along the  $CC'$  cross section given in Figure 9c suggests that a strong uplifting in the WAFZ with a high  $\theta_e$  layer extended from the coast to the study region (up to 3 km), but sharply dropped beneath the warm front in the north region. Taylor and Guymer [1983] also found high  $\theta_e$  values and strong turbulence mixing in the WAFZ. In fact, the elevated PBL height given in Figure 9c (see the black line) also agrees with that finding and indicates good dispersion of air pollution within the WAFZ. The projected flight track on the cross section in Figure 9c further suggests that our aircraft study successfully crossed through different air mass zones over the warm front, and the flight at the altitude of 2.6 km was taken within the WCB circulation (i.e., WCB1) above the frontal zone.

#### 4.4. Lagrangian Perspective on the Pollution Source

##### 4.4.1. Results for the Background and Polluted Air Parcels

[29] To diagnose and analyze the possible source regions of the observed air pollutants, we applied the Lagrangian particle dispersion model, FLEXPART, in a backward mode. We first focus on the polluted air and compare it with background air parcel to show how the Lagrangian simulation was conducted and to understand the difference in transport processes and/or sources for the two cases.

[30] Figures 10a and 10d give the distributions of the normalized residence time (i.e., retroplume) column of particles arriving in the small segments ( $0.1^\circ \times 0.1^\circ \times 200$  m) for the background and polluted air parcels, respectively. Figures 10b and 10e show the retroplume in the footprint layer (i.e., below 100 m), and Figures 10c and 10f present the simulated potential source contribution map, i.e., CO mixing ratio contributions (in units of ppbv) in each grid cell (with a horizontal resolution of  $0.1^\circ$ ) in east Asia for the two cases, respectively.

[31] For the background air, Figure 10a shows that the air masses mainly originated from the Mongolian Plateau and passed over the northern edge of the NCP before being transported to the sampling location. The narrow belt of retroplume of the latest history suggests a weak dispersion during the free-tropospheric advection from the NCP to

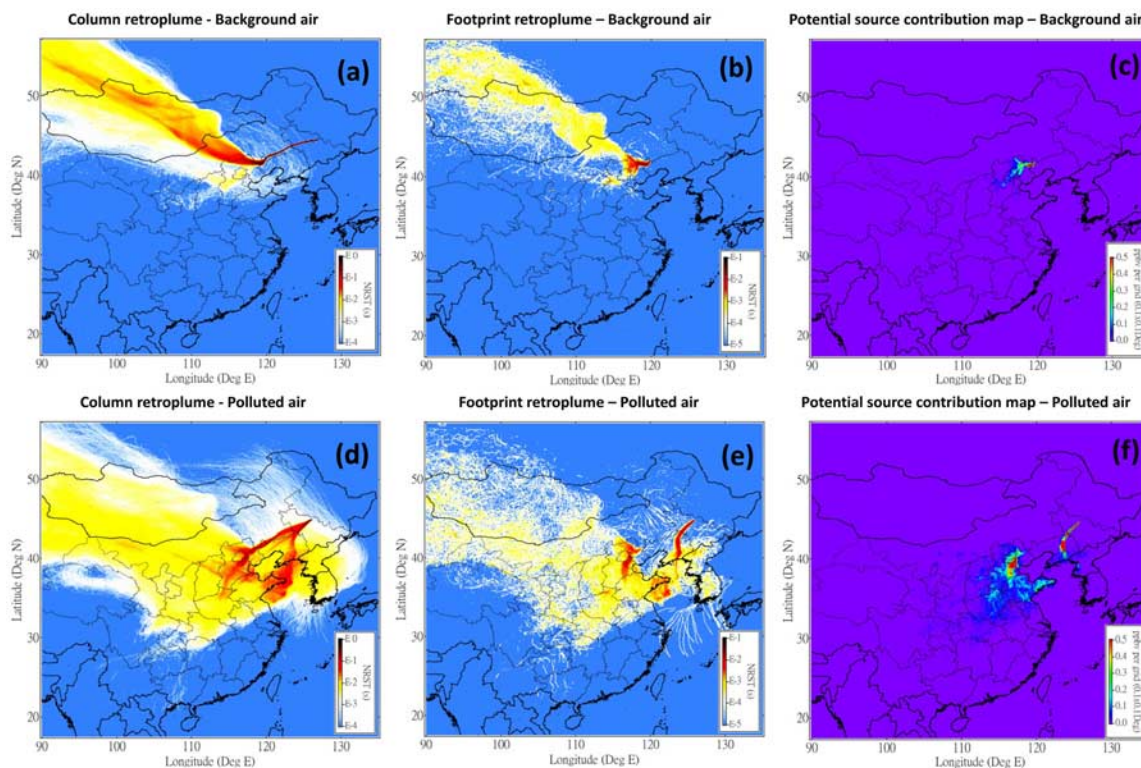


**Figure 10.** Distributions of the (a and d) column retroplume field, (b and e) footprint retroplume, and (c and f) potential source contribution map of CO for the small receptor segments ( $0.1^\circ \times 0.1^\circ \times 200\text{ m}$ ) of background (1510 LT) and polluted (1530 LT) air parcels, respectively. Note that the horizontal resolution is  $0.1^\circ$ .

the sampling location. The footprint retroplume given in Figure 10b does show that the air spent less time in the PBL. For the polluted air, the transport pathway of the air masses was different from the previous one. The air masses had a longer residence time over north China, especially over the NCP (Figure 10d). The column retroplume also shows two branches with one transport northeastward from the northern part of the NCP, i.e., around the Beijing and Tianjin city clusters, and another from the southeastern part of the NCP and passing over Liaoning. Figure 10e reveals that the former branch had a high footprint residence time around the Beijing-Tianjin area but was not in contact with the surface afterward. The potential source contribution maps (see section 3.2) clearly show that for background air, only the northeastern edge of the NCP made some contribution to the observations, but for polluted air, the emissions along the transport pathways in Jinlin, Liaoning, and the whole NCP, especially the Beijing-Tianjin areas (see the hot spots in Figure 10f) had strong impacts on the observed high CO concentrations.

[32] Further analysis suggests that the plumes from the northern part of the NCP were associated with the frontal activities over this region. As mentioned, the stagnant front, located at the northern edge of the NCP from noontime 25 June to early morning 26 June, contributed to the lifting of air pollution there. This is also consistent with the convective lifting around NCP shown in Figure 7b. An age spectrum analysis of the northern NCP plumes in section 4.4.3 consistently shows a transport time of 1 to 2 days from this region to the aircraft sampling location. To

help understand the transport processes related to the pollution ventilation there, we show the averaged surface wind streamlines from 1200 LT on 25 June to 0600 LT on 26 June superimposed with the satellite cloud image at 2000 LT on 25 June in Figure 11. It can be seen that during this 18-hour period, there was a strong convergence band corresponding with clouds along the front, and the clouds were more convective over the mountains to the north of Beijing (see the topographical contour). Many studies [e.g., Henne *et al.*, 2004, 2005; Rotach and Zardi, 2007] have shown that the topographic venting effect can play an important role in PBL-FT air pollution transport, and Ding *et al.* [2008] also mentioned the possible influence of the mountains in the northern part of the NCP on the vertical transport of air pollution. For the present study, we believe that the stagnant front was the main contributor, providing a strong and continuous northeastward surface advection in the warm sector, but that the topography aided or enhanced the convection and pollution venting.

#### 4.4.2. Potential Source Contribution Analysis

[33] For the potential source contribution maps of CO given in Figures 10c and 10f, a sum of the values at all grids gives the total simulated CO mixing ratios of the sampling boxes. Using the same method, we did a simulation every 10 min during the entire flight (26 sample boxes in total), and give the time series of the simulated CO, apportioned into age spectra, and the observations in Figure 12. Because the 7-day backward simulation can account only for the emissions during the previous week, we assume a unified background CO of 75 ppbv during the entire flight.

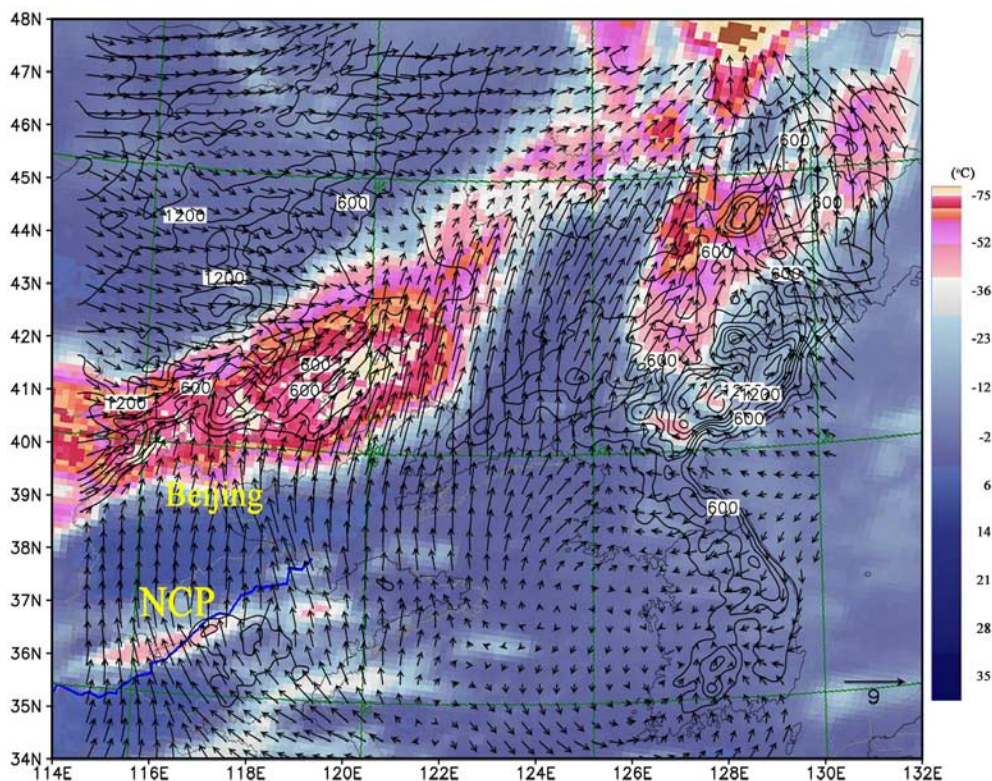


**Figure 11.** Averaged surface (10 m) wind vectors (from 1200 LT on 25 June to 0600 LT on 26 June), superimposed with the FY-2 satellite IR cloud image at 2000 LT on 25 June (i.e., same as Figure 6a) and topographical height (contour lines are given in units of meters).

[34] A comparison of the overall simulations with the observations shows that FLEXPART overestimated the CO mixing ratio during the 1400–1450 LT and 1700–1730 LT periods, but underestimated the peaks around 1500 LT. For the whole flight, the RMS difference is 194 ppbv. The disagreement between simulations and observations could be due to the uncertainty in mesoscale simulation and processing of emissions. As our flight was taken around the top of the PBL, with a strong air pollution gradient, it was difficult to capture exactly detailed variations during the flight. Since our emission data did not include biomass burning, which has been found active in June in NCP [e.g., Wang *et al.*, 2004; Ding *et al.*, 2008], this can also cause some uncertainty. However, by examining satellite fire products (<http://firefly.geog.umd.edu/firemap/>) we found little biomass burning in the upwind areas during 20–27 June (figure not shown). We believe the relatively low resolution ( $0.5^\circ$ ) and the fact that we did not account for temporal variation and plume rise of the elevated point sources could be other possible causes of uncertainty. Furthermore, it should be noted that CO is not a completely inert tracer but also can be from oxidation of hydrocarbons. Nevertheless, the simulation has captured the general variation pattern of CO, and the general source analysis of the time series is helpful in identifying the transport mechanisms.

[35] The age spectrum given in Figure 12 shows that most of the air pollutants (up to 67%) were emitted during the last three days, especially the second-to-last day. This suggests that the sample air masses were photochemically aged,

consistent with the high ozone concentration and positive correlation between the primary and secondary pollutants. With the source category classification of the emission inventory, we also found that industrial emissions contributed the largest proportion ( $\sim 45\%$ ) of the CO during the entire episode (figure not shown).

#### 4.4.3. Regional Contributions and a Linkage to the Transport Mechanisms

[36] As discussed, the emission characteristics in the local and upwind regions were quite different. To further understand the relative contributions of emissions from these regions to the observations, we calculated the contributions of CO from four areas: the provinces of Jilin and Liaoning and the northern part of the NCP, containing the province of Hebei and Beijing-Tianjin city clusters, and the southern part of the NCP, including the province of Shandong and the northern part of the province of Jiangsu (see Figure 1a for the definition). It should be noted that here the NCP is a broad definition, covering the plain area in the north and east of China.

[37] For each area, the simulated time series for CO with the age spectrum and percentage of total (as in Figure 12) along the flight track are presented in Figures 13a–13d, respectively. Figures 13a–13d clearly show the impacts from sources in these regions with different transport age. With low anthropogenic emissions, Jilin contributed a small part of the CO that was emitted during the last day (3.2% in average). The upwind adjacent province, Liaoning, contributed quite a large part of CO in the ascent and descent stage and peak of the polluted air, and most of the peaks also had

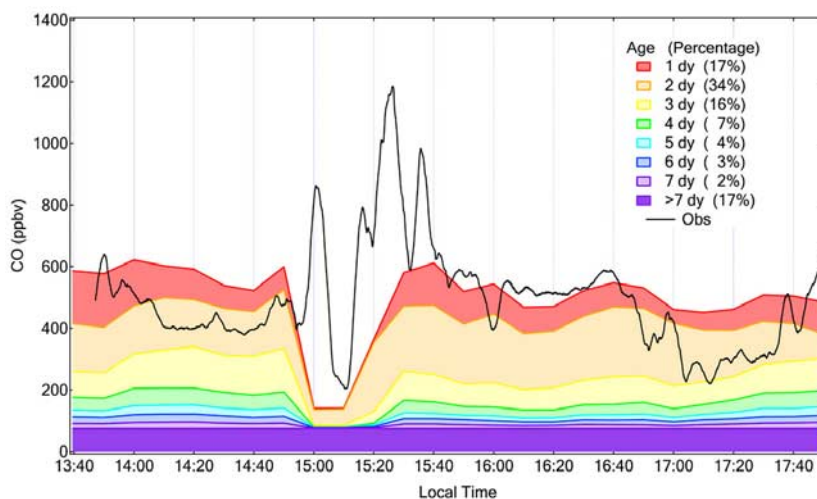


**Figure 12.** Time series of the observed CO and simulated CO age spectrum and percentage of total obtained from FLEXPART simulations. Note that a 75 ppbv background level of CO was assumed.

an age of one day ( $\sim 13.5\%$ ), revealing fast northeastward transport and a strong upward mixing within the PBL. The emissions in the northern part of the NCP contributed the most CO during the entire period, especially when the aircraft flew at higher altitudes, i.e., from 1510 LT to 1640 LT. A calculation using emissions from Beijing and Tianjin alone suggested a pattern similar to that of Figure 13c, but the values were about half those of the entire northern part of the NCP (figure not shown). This result reveals the important impact of the two mega-cities for this episode. The age spectrum in Figure 13c suggests that the northern NCP plumes (up to 20.4%) were between 1 to 2 days old, consistent with the period of the existence of the front over

this region, as discussed previously (i.e., Figure 11). Figure 13d suggests a relatively uniform contribution from the southern part of the NCP, except when the aircraft crossed the dry intrusion, i.e., the background air parcel. The age spectrum shows that the air masses from this region were relatively more aged (2–3 days). In summary, these results confirm the important contribution of anthropogenic emissions in the NCP and reveal two different transport pathways: the southern air masses were slowly transported within the low PBL to NE China, but the northern ones were more quickly transported after frontal/topographic venting.

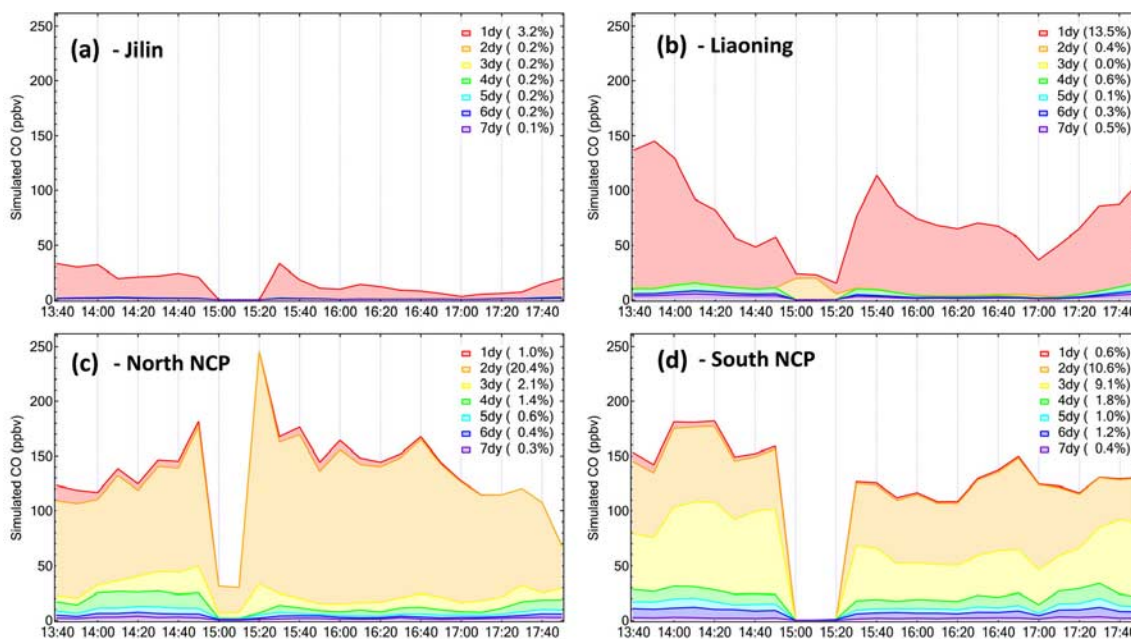


**Figure 13.** Same as Figure 12 but counting only emissions from the four areas: (a) Jilin, (b) Liaoning, (c) northern part of the NCP, and (d) southern part of the NCP (see Figure 1a for the definition of the four areas).

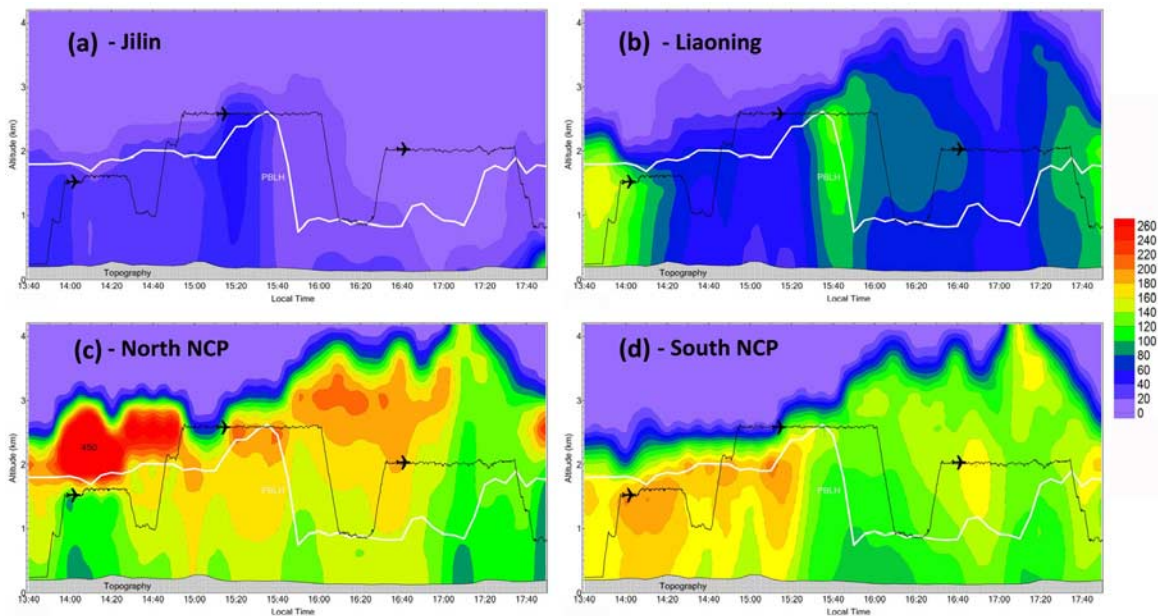


**Figure 14.** Vertical cross section of CO source contributions (units are ppbv) on the curtain along the flight track from different areas: (a) Jilin, (b) Liaoning, (c) northern part of the NCP, and (d) southern part of the NCP.

[38] To better understand the regional contributions to the vertical distribution of CO concentrations and further link them to the transport mechanisms for pollution from different regions, in Figures 14a–14d we present the CO contributions from the four areas (as in Figure 13) at different altitudes on the curtain along the flight track. Figures 14a–14d give a 3-D perspective of the CO source contributions from the different regions. For Jilin, the CO distributions were related more to the change in the PBL height and generally show a constant distribution within the PBL, suggesting that vertical turbulence mixing plays a major role in redistributing local emissions. Regarding the air masses from the adjacent upwind province, Liaoning (Figure 14b), relatively high CO concentrations existed within the PBL during the ascent and descent stages, but an obvious PBL-FT transport event appeared around 1540 LT, i.e., in the front of the WAFZ. As for the air pollution from the northern part of the NCP (Figure 14c), high CO concentration appeared in the free troposphere (up to 450 ppbv) around 1400 LT and later within the WAFZ. The high regional CO plume in the early stage, the center of which was not actually captured by the aircraft, corresponded with the frontal/topographic ventilation, which, as mentioned above, occurred at the northern edge of the NCP 1 to 2 days before the measurement. The plumes lifted up to 4 km in the late stage were related to the ascent of the WCB and well mixed within the WAFZ. Figure 14c also suggests that an interesting entrainment of pollution from the FT into the PBL appeared around 1500 LT, accompanied by the dry intrusion of free tropospheric background air. The CO tracer from the southern part of the NCP (Figure 14d) showed a different transport mechanism. Because the air mass was transported within the PBL and experienced a longer transport time, the air pollutants were well mixed in the early stage (from 1340 to 1520 LT), but

thereafter experienced the same uplifting by the WCB and WAFZ in the north.

#### 4.5. Implications of the Environmental Impact of This Case

[39] As mentioned in the introduction, the study of midlatitude cyclones and their associated fronts and WCB circulations is important because of their significant roles in lifting PBL air pollutants into the FT and the subsequent long-range transport of such pollutants. It is very important to understand cross-boundary transport and the regional, even global, impact of high emissions from the polluted region in north China.

[40] Previous analysis and discussion, especially of the transport patterns of regional emissions, suggest that the NCP plumes can be transported to NE China, via slow transport in the PBL or fast transport in the FT, and consequently be entrained down to the surface. Photochemical pollution has been found in north China [Wang *et al.*, 2006; Ding *et al.*, 2008], and its potential impact on agriculture in NE China via long distance transport needs to be investigated because NE China is one of the key agricultural bases in China and most of the crops there are planted in summer.

[41] Regarding the important roles of WCBs in continental or global transport of air pollution, it would be interesting to see the possible long-distance impact of aircraft-sampled regional air pollution. Figure 15 gives the 10-day forward trajectories for the matrix of points at 1500 m and 2500 m over the study region at 1600 LT on 27 June to show the pathways of the sampled air masses in the subsequent period. As the WRF simulations cover only east Asia, here the trajectories were calculated using HYSPLIT with hourly WRF output, nested with three-hourly data from the Global Data Assimilation System Archive of the

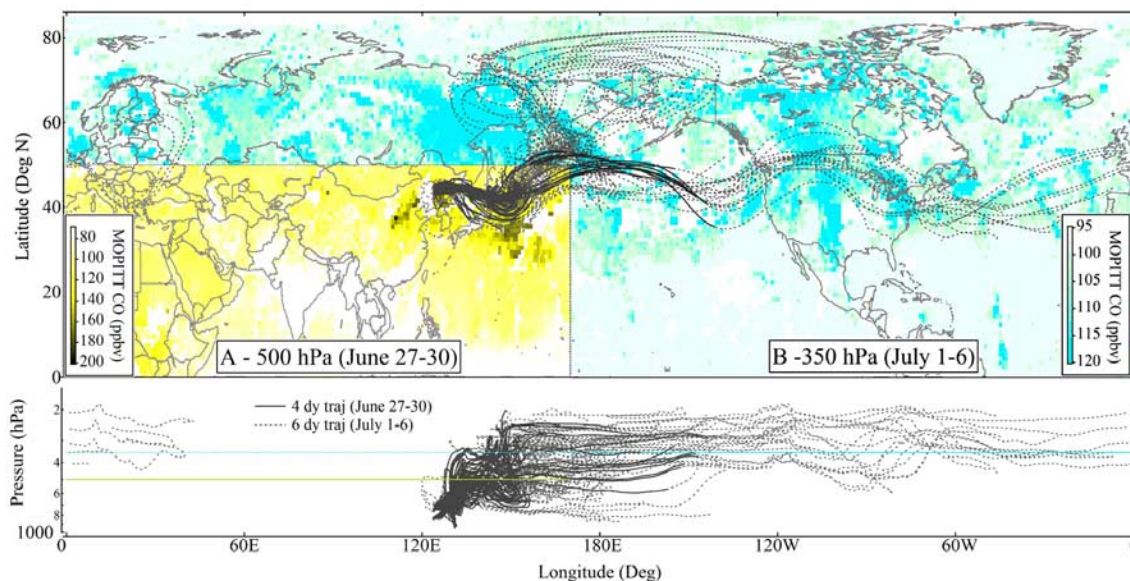


**Figure 15.** Ten-day forward trajectories starting at the matrix of points at 1500 and 2500 m over the aircraft study region at 1600 LT on 27 June and MOPITT satellite retrieval CO mixing ratio. The black solid lines and gray dashed lines show the trajectories for 27–30 June and 1–6 July, respectively. (a) Averaged 500 hPa MOPITT CO for 27–30 June; (b) averaged 350 hPa MOPITT CO for 1–6 July.

NCEP with a resolution of 1 degree (see <http://www.ready.noaa.gov/ss/transport/gdas1.html>). The trajectories given in Figure 15 suggest that the air mass ascended mostly to a level of 500 hPa on average during the first four days (i.e., 27–30 June; see the black lines), and in the latter six days (see the dashed gray line) was lifted into the upper troposphere (at around the 350 hPa level). Considering the difference in the mean altitudes of the trajectories, in Figure 15, the averaged 500 hPa MOPITT CO during the first period and the 350 hPa one during the second period are shown in frames A and B, respectively. Examination of the averaged CO map helps us to understand the plume track during a period as the transport of a plume of very high concentrations should leave a belt-like track on the averaged map.

[42] Interestingly, Figure 15 does show some agreement between the forward trajectory and CO distribution. For example, CO showed two branches of plumes in the east of north Japan (i.e., around the upper right corner of frame A), with one transported to the Arctic region in the north and another one over the Pacific, extending to the west and even east coast of North America. Though the MOPITT CO concentrations in the downwind areas were much lower than our measurements because of mixing and dilution in the air, a significant enhancement of the concentrations can be clearly seen in these plume belts. It should be noted that the plume concentrations, in fact, might be several times higher than those shown in Figure 15 because the multiple-day average could smooth/weaken the peak. These results further suggest that because of strong advection, vented regional pollutants can be transported over long distances and have significant impacts on the chemical component of the upper troposphere over the Pacific, the Arctic, or even globally [Stohl *et al.*, 2003, 2007; Cooper *et al.*, 2004]. For this aircraft case, it is particularly important that the flight was conducted in the initial stage of the WCB, and that the sampled pollution plumes were further lifted by

the developing WCB and exported from Asia. As mentioned, previous studies of the climatological occurrence of cyclones [Chen *et al.*, 1991] and WCBs [Stohl, 2001; Eckhardt *et al.*, 2004] have suggested a very high frequency of cyclogenesis/cyclone events and WCBs in east Asia, particularly over the NCP in the summer. Giving a detailed dynamic analysis and the transport mechanisms for such a case, our study further highlights the important role of midlatitude cyclones in exporting air pollution from this region in warm seasons.

## 5. Conclusions

[43] Aircraft measurements were carried out in NE China in June 2007 to investigate the transport characteristics, and gain a better understanding of the regional impact, of photochemical plumes from the North China Plain under the influence of a midlatitude cyclone. Synoptic analysis, comprehensive mesoscale meteorological modeling, and Lagrangian simulations were carried out to help in the understanding of the atmospheric dynamics and transport mechanisms, particularly the PBL-FT transport, in the region adjacent to the warm front and within the WCB circulations. Our conclusions are listed below.

[44] 1. In situ measurements show regional-scale high photochemical pollution in the PBL and FT in NE China on 27 June 2007, with O<sub>3</sub> concentration up to 140 ppb and CO and SO<sub>2</sub> concentrations over 1185 ppbv and 14.6 ppbv, respectively, at an altitude of 2.6 km. The measurements, with positive correlations between the primary and secondary trace gases and aerosol light scattering coefficient, suggest that the aircraft sampled photochemically aged air masses during the entire flight.

[45] 2. Synoptic-scale analysis with WRF output and satellite images suggests that our study was conducted in the warm sector of a midlatitude cyclone in north China.

The aircraft measurements captured the WCB circulation and the WAFZ over the warm front of the cyclone, with the air masses transported from the southwest and further lifted over the front and to higher altitudes by the WCB. PBL structure analysis suggests that the PBL over this region strongly interacted with the front and the WAFZ.

[46] 3. The backward Lagrangian simulations with WRF/FLEXPART captured well the different transport processes and characteristics of the observed CO variations, and show the advantage of tracing the potential source regions and understanding the regional contributions for field observations. The emissions from Liaoning and the NCP were generally transported to the study area after a transport period of 1 to 3 days, and contributed to the majority of the observed CO plumes. The observed high air pollution in the FT mostly originated from the NCP, especially from the northern part of the NCP including the megacities Beijing and Tianjin, where the plumes were vented into the FT by a stagnant front, probably with the aid of topographical lifting and subsequently advected to the study region within 1 to 2 days. The plumes mixed with the pollution from the southern part of the NCP and Liaoning, which was transported within the PBL and lifted to a high altitude by the WAFZ and the developing WCB, and subsequently transported to the upper troposphere and exported from Asia.

[47] 4. The study highlights the important role of midlatitude cyclones in exporting NCP photochemical plumes in the summer and the potential impact on agriculture in NE China and the chemical composition of the middle and upper troposphere on a continental, even global, scale.

[48] **Acknowledgments.** We would like to thank Steven Poon and Changshu Mi for their contribution in mounting the aircraft instruments. We thank the aircraft crew, especially Colonel Kuilin Li, for their cooperation and support during the aircraft campaign. We thank Yong Yu for the meteorological forecasting service for the experiment, Zhilai Shen for developing the sample inlets, and Yuxia Wu for helpful discussions. We also thank Jerome Fast of the National Center for Atmospheric Research for the development and release of FLEXPART for WRF. We also thank two anonymous referees for their very helpful suggestions which have improved the presentation of this paper. This work was funded by the National Basic Research Program (973 Project 2005CB422203) and Hong Kong Polytechnic University (G-YX86 and 1-BB94).

## References

- Bethan, S., et al. (1998), Chemical air mass differences near fronts, *J. Geophys. Res.*, *103*, 13,413–13,434, doi:10.1029/98JD00535.
- Bolton, D. (1980), The computation of equivalent potential temperature, *Mon. Weather Rev.*, *108*, 1046–1053, doi:10.1175/1520-0493(1980)108<1046:TCOEPT>2.0.CO;2.
- Carlson, T. N. (1998), *Mid-Latitude Weather Systems*, Am. Meteorol. Soc., Boston, Mass.
- Chatfield, R. B., and P. J. Crutzen (1984), Sulfur-dioxide in remote oceanic air: Cloud transport of reactive precursors, *J. Geophys. Res.*, *89*, 7111–7132, doi:10.1029/JD089iD05p07111.
- Chen, S. J., Y. H. Kuo, P. Z. Zhang, and Q. F. Bai (1991), Synoptic climatology of cyclogenesis over east Asia, 1958–1987, *Mon. Weather Rev.*, *119*, 1407–1418, doi:10.1175/1520-0493(1991)119<1407:SCOCOE>2.0.CO;2.
- Chin, M., et al. (1994), Relationship of ozone and carbon monoxide over North America, *J. Geophys. Res.*, *99*, 14,565–14,573, doi:10.1029/94JD00907.
- Cooper, O. R., et al. (2001), Trace gas signatures of the airstreams within North Atlantic cyclones: Case studies from the North Atlantic Regional Experiment (NARE '97) aircraft intensive, *J. Geophys. Res.*, *106*, 5437–5456, doi:10.1029/2000JD900574.
- Cooper, O. R., et al. (2004), A case study of transpacific warm conveyor belt transport: Influence of merging airstreams on trace gas import to North America, *J. Geophys. Res.*, *109*, D23S08, doi:10.1029/2003JD003624.
- Cooper, O. R., et al. (2006), Large upper tropospheric ozone enhancements above midlatitude North America during summer: In situ evidence from the IONS and MOZAIC ozone measurement network, *J. Geophys. Res.*, *111*, D24S05, doi:10.1029/2006JD007306.
- Crawford, J. H., et al. (2004), Relationship between Measurements of Pollution in the Troposphere (MOPITT) and in situ observations of CO based on a large-scale feature sampled during TRACE-P, *J. Geophys. Res.*, *109*, D15S04, doi:10.1029/2003JD004308.
- de Foy, B., J. R. Varela, L. T. Molina, and M. J. Molina (2006), Rapid ventilation of the Mexico City basin and regional fate of the urban plume, *Atmos. Chem. Phys.*, *6*, 2321–2335.
- Delene, D. J., and J. A. Ogren (2002), Variability of aerosol optical properties at four North American surface monitoring sites, *J. Atmos. Sci.*, *59*, 1135–1150, doi:10.1175/1520-0469(2002)059<1135:VOAOPA>2.0.CO;2.
- Dickerson, R. R., et al. (2007), Aircraft observations of dust and pollutants over northeast China: Insight into the meteorological mechanisms of transport, *J. Geophys. Res.*, *112*, D24S90, doi:10.1029/2007JD008999.
- Ding, A., et al. (2004), Simulation of sea-land breezes and a discussion of their implications on the transport of air pollution during a multi-day ozone episode in the Pearl River Delta of China, *Atmos. Environ.*, *38*, 6737–6750, doi:10.1016/j.atmosenv.2004.09.017.
- Ding, A. J., et al. (2008), Tropospheric ozone climatology over Beijing: Analysis of aircraft data from the MOZAIC program, *Atmos. Chem. Phys.*, *8*, 1–13.
- Donnell, E. A., D. J. Fish, E. M. Dicks, and A. J. Thorpe (2001), Mechanisms for pollutant transport between the boundary layer and the free troposphere, *J. Geophys. Res.*, *106*, 7847–7856, doi:10.1029/2000JD900730.
- Eckhardt, S., et al. (2004), A 15-year climatology of warm conveyor belts, *J. Clim.*, *17*, 218–237, doi:10.1175/1520-0442(2004)017<0218:AYCOWC>2.0.CO;2.
- Gao, J., T. Wang, A. J. Ding, and C. B. Liu (2005), Observational study of ozone and carbon monoxide at the summit of mount Tai (1534m a.s.l.) in central-eastern China, *Atmos. Environ.*, *39*, 4779–4791, doi:10.1016/j.atmosenv.2005.04.030.
- Henne, S., et al. (2004), Quantification of topographic venting of boundary layer air to the free troposphere, *Atmos. Chem. Phys.*, *4*, 497–509.
- Henne, S., et al. (2005), Influence of mountain venting in the Alps on the ozone chemistry of the lower free troposphere and the European pollution export, *J. Geophys. Res.*, *110*, D22307, doi:10.1029/2005JD005936.
- Holton, J. R. (2004), *An Introduction to Dynamic Meteorology*, 4th ed., Elsevier, New York.
- Jacob, D. J., et al. (2003), Transport and Chemical Evolution over the Pacific (TRACE-P) aircraft mission: Design, execution, and first results, *J. Geophys. Res.*, *108*(D20), 9000, doi:10.1029/2002JD003276.
- Jaegle, L., et al. (2003), Sources and budgets for CO and O-3 in the north-eastern Pacific during the spring of 2001: Results from the PHOBEA-II Experiment, *J. Geophys. Res.*, *108*(D20), 8802, doi:10.1029/2002JD003121.
- Jaffe, D., et al. (1999), Transport of Asian air pollution to North America, *Geophys. Res. Lett.*, *26*, 711–714, doi:10.1029/1999GL900100.
- Jaffe, D., I. McKendry, T. Anderson, and H. Price (2003), Six “new” episodes of trans-Pacific transport of air pollutants, *Atmos. Environ.*, *37*, 391–404, doi:10.1016/S1352-2310(02)00862-2.
- Kiley, C. M., and H. E. Fuelberg (2006), An examination of summertime cyclone transport processes during intercontinental chemical transport experiment (INTEX-A), *J. Geophys. Res.*, *111*, D24S06, doi:10.1029/2006JD007115.
- Li, J., et al. (2007), Modeling study of ozone seasonal cycle in lower troposphere over east Asia, *J. Geophys. Res.*, *112*, D22S25, doi:10.1029/2006JD008209.
- Liang, Q., et al. (2004), Long-range transport of Asian pollution to the northeast Pacific: Seasonal variations and transport pathways of carbon monoxide, *J. Geophys. Res.*, *109*, D23S07, doi:10.1029/2003JD004402.
- Liu, H. Y., et al. (2003), Transport pathways for Asian pollution outflow over the Pacific: Interannual and seasonal variations, *J. Geophys. Res.*, *108*(D20), 8786, doi:10.1029/2002JD003102.
- Luke, W. T., et al. (1992), Tropospheric chemistry over the lower Great Plains of the United States: 2. Trace gas profiles and distributions, *J. Geophys. Res.*, *97*, 20,647–20,670.
- Malm, W. C., et al. (2003), Humidity-dependent optical properties of fine particles during the Big Bend regional aerosol and visibility observational study, *J. Geophys. Res.*, *108*(D9), 4279, doi:10.1029/2002JD002998.
- Mari, C., et al. (2004), Export of Asian pollution during two cold front episodes of the TRACE-P experiment, *J. Geophys. Res.*, *109*, D15S17, doi:10.1029/2003JD004307.

- Miyazaki, Y., et al. (2003), Synoptic-scale transport of reactive nitrogen over the western Pacific in spring, *J. Geophys. Res.*, *108*(D20), 8788, doi:10.1029/2002JD003248.
- Oshima, N., et al. (2004), Asian chemical outflow to the Pacific in late spring observed during the PEACE-B aircraft mission, *J. Geophys. Res.*, *109*, D23S05, doi:10.1029/2004JD004976.
- Palau, J. L., et al. (2006), A study of dispersion in complex terrain under winter conditions using high-resolution mesoscale and Lagrangian particle models, *Atmos. Chem. Phys.*, *6*, 1105–1134.
- Parrish, D. D., et al. (1993), Export of North American ozone pollution to the North Atlantic Ocean, *Science*, *259*, 1436–1439, doi:10.1126/science.259.5100.1436.
- Rotach, M. W., and D. Zardi (2007), On the boundary-layer structure over highly complex terrain: Key findings from MAP, *Q. J. R. Meteorol. Soc.*, *133*, 937–948, doi:10.1002/qj.71.
- Ryan, W. F., R. R. Dickerson, G. J. Huffman, and W. T. Luke (1992), Tropospheric chemistry over the lower Great Plains of the United States: 1. Meteorology, *J. Geophys. Res.*, *97*, 17,963–17,984.
- Schultz, D. M. (2001), Reexamining the cold conveyor belt, *Mon. Weather Rev.*, *129*, 2205–2225, doi:10.1175/1520-0493(2001)129<2205:RTCCB>2.0.CO;2.
- Seibert, P., and A. Frank (2004), Source-receptor matrix calculation with a Lagrangian particle dispersion model in backward mode, *Atmos. Chem. Phys.*, *4*, 51–63.
- Skamarock, W. C., et al. (2005), *A Description of the Advanced Research WRF Version 2*, Natl. Cent. for Atmos. Res., Boulder, Colo.
- Stohl, A. (2001), A 1-year Lagrangian “climatology” of airstreams in the Northern Hemisphere troposphere and lowermost stratosphere, *J. Geophys. Res.*, *106*, 7263–7279, doi:10.1029/2000JD900570.
- Stohl, A., and T. Trickl (1999), A textbook example of long-range transport: Simultaneous observation of ozone maxima of stratospheric and North American origin in the free troposphere over Europe, *J. Geophys. Res.*, *104*, 30,445–30,462, doi:10.1029/1999JD900803.
- Stohl, A., et al. (2003), A backward modeling study of intercontinental pollution transport using aircraft measurements, *J. Geophys. Res.*, *108*(D12), 4370, doi:10.1029/2002JD002862.
- Stohl, A., et al. (2005), Technical note: The Lagrangian particle dispersion model FLEXPART version 6.2, *Atmos. Chem. Phys.*, *5*, 2461–2474.
- Stohl, A., et al. (2007), Aircraft measurements over Europe of an air pollution plume from Southeast Asia—Aerosol and chemical characterization, *Atmos. Chem. Phys.*, *7*, 913–937.
- Streets, D. G., et al. (2006), Revisiting China’s CO emissions after the Transport and Chemical Evolution over the Pacific (TRACE-P) mission: Synthesis of inventories, atmospheric modeling, and observations, *J. Geophys. Res.*, *111*, D14306, doi:10.1029/2006JD007118.
- Taylor, P. K., and T. H. Guymer (1983), The structure of an atmospheric warm front and its interaction with the boundary layer, *Philos. Trans. R. Soc. London Ser. A*, *308*, 341–358.
- Tsutsumi, Y., Y. Makino, and J. B. Jensen (2003), Vertical and latitudinal distributions of tropospheric ozone over the western Pacific: Case studies from the PACE aircraft missions, *J. Geophys. Res.*, *108*(D8), 4251, doi:10.1029/2001JD001374.
- Vaughan, G., W. E. Garland, D. J. Dewey, and C. Gerbig (2003), Aircraft measurements of a warm conveyor belt—A case study, *J. Atmos. Chem.*, *46*, 117–129, doi:10.1023/A:1026025516092.
- Wang, T., T. F. Cheung, M. Anson, and Y. S. Li (2001), Ozone and related gaseous pollutants in the boundary layer of eastern China: Overview of the recent measurements at a rural site, *Geophys. Res. Lett.*, *28*, 2373–2376, doi:10.1029/2000GL012378.
- Wang, T., et al. (2004), Relationships of trace gases and aerosols and the emission characteristics at Lin’an, a rural site in eastern China, during spring 2001, *J. Geophys. Res.*, *109*, D19S05, doi:10.1029/2003JD004119.
- Wang, T., A. J. Ding, J. Gao, and W. S. Wu (2006), Strong ozone production in urban plumes from Beijing, China, *Geophys. Res. Lett.*, *33*, L21806, doi:10.1029/2006GL027689.
- Wernli, H., and H. C. Davies (1997), A Lagrangian-based analysis of extratropical cyclones: 1. The method and some applications, *Q. J. R. Meteorol. Soc.*, *123*, 467–489, doi:10.1002/qj.49712353811.
- Wild, O., and H. Akimoto (2001), Intercontinental transport of ozone and its precursors in a three-dimensional global CTM, *J. Geophys. Res.*, *106*, 27,729–27,744, doi:10.1029/2000JD000123.
- A. Ding, J. Gao, Y. Ren, T. Wang, X. Wei, and L. Xue, Department of Civil and Structural Engineering, Hong Kong Polytechnic University, Hung Hom, Kowloon, Hong Kong, China. (cetwang@polyu.edu.hk)
- D. Jin, J. Liu, and Y. Qi, Weather Modification Office, Jilin Provincial Meteorological Bureau, 653 Hepingdajie Road, Changchun, Jilin, 130062, China.
- H. Lei and X. Zhang, Institute of Atmospheric Physics, Chinese Academy of Science, Beijing, 100029, China.
- A. Stohl, Norwegian Institute for Air Research, Instituttveien 18, N-2027 Kjeller, Norway.
- X. Wang, Chinese Research Academy of Environmental Sciences, 8 Dayangfang BeiYuan Road, Chaoyang District, Beijing, 100012, China.